International Journal of Catalysis and Chemical Engineering
ISSN: 3068-9368

PRIME OPEN ACCESS

Volume 1, Issue 2

Research Article

Date of Submission: 26 Aug, 2025
Date of Acceptance: 22 September, 2025
Date of Publication: 30 September, 2025

Multiphoton Absorption, Generation Of Higher Order Harmonics And Strong Blue - Emission From The Ultrasmall Upconverting Nanoparticles

Monami Das Modak[1,2*], Pradip Paik[3], Anil K Chaudhury[4] and Nabanita Pal[1]

[1]Department of Physics and Chemistry, Mahatma Gandhi Institute of Technology (MGIT), India

[2]School of Engineering Sciences and Technology, University of Hyderabad, India

[3]School of Biomedical Engineering, Indian Institute of Technology (IIT)-BHU, Varanasi, India

[4]Advanced Center of Research in High Energy Materials, University of Hyderabad, India

***Corresponding Author:**
Monami Das Modak, Department of Physics and Chemistry, Mahatma Gandhi Institute of Technology (MGIT), India.

Citation: Modak, M. D., Paik, P., Chaudhury. A. K., Pal, N. (2025). Multiphoton Absorption, Generation Of Higher Order Harmonics And Strong Blue - Emission From The Ultrasmall Upconverting Nanoparticles. *Int J Catalysis Chem Eng, 1*(2), 01-09.

Abstract
Erbium, Ytterbium doped sodium yttrium fluoride nanocrystals (NaYF4:Yb3+ /Er3+) are promising candidates to be considered as the highly efficient upconverting nanomaterials. Herein, the generation of efficient higher order harmonics by five, four photon absorption processes (Multiphoton absorption- MPA) are revealed under the excitation with femtosecond-laser (fs-laser) with 140 fs-laser pulses in NaYF4: Yb3+/Er3+ ultrasmall upconverting nanoparticles (US-UCNPs; sub-5nm) at room temperature. These US-UCNPs were prepared following thermal decomposition procedure. The generation of fourth order harmonic peak (FHG) and fifth order harmonic peak (FIHG) are distinguished under fs- pulse excitation, concurrently. Further, the precisely synthesized US-UCNPs exhibit strong blue emissions under 900 nm continuous wave (CW) laser-diode excitation. A significant red shifting is explored with 950-990 nm tunable laser sources.

Keywords: Ultrasmall UCNPs, MPA, Fs-Lasing Up Conversion, Higher Order Harmonics

Toc Graphics

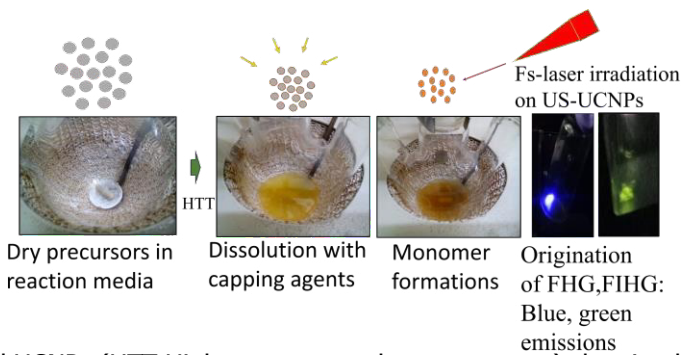

TOC. The prepared Ultrasmall UCNPs (HTT-High temperature heat treatment) showing bright blue and green visible UC-emissions and produce higher order upconversion lasing while interacted with 950-980nm tunable fs-laser.

Introduction

The unique photophysical properties of upconverting nanoparticles (UCNPs) promote them for being intensely used in biomedical fields [1,2]. The tuned emissions from them by irradiating with NIR photons have already been applied in a diverse range of applications – solar cells, display systems, drug delivery, photodynamic therapy and obviously in bio-imaging, biolabeling [2–7]. Researchers have also designed different-sized UCNPs to observe their energy absorbing and transferring mechanism and then to make them suitable candidate for several purposes [1,2]. However, for in-vivo uses, very small 'stealth' nanoparticles (sub:8-10nm) are particularly important because they can circulate inside the body without being detected by the immune system, therefore, fabricating such particles comprising a defined ultrasmall sizes with the required optical properties remains a challenging aspect to us and to the best of our knowledge, this aspect is in its infancy.

The upconversion phenomenon is basically a minimum of two-photon involved process exhibiting bright luminescence via intra 4f or 4f-5d transitions. The other properties like long emission life-time, large – antistokes shift, tuned emission wavelengths with tuning sizes by choosing proper host materials incorporated with suitable synthetic approaches and spectroscopic properties make them unique. On the other side, as we know most of the chlorides and bromides are moisture sensitive and are not suitable for bio-labeling whereas rare-earth (RE) fluorides (REF3, AREF4; A=Alkali metals) owing to their high refractive index, high transparency raised from low-energy phonons – have been considered as excellent host materials for preparing UCNPs. It is well known to us that, those UCNPs get excited by low-energy photons (NIR-light) which undergoes NIR-visible/ultraviolet conversion processes to release high-energy photons. This fact overcomes the limitations (conversion of UV- visible light to NIR/IR radiation involve with photodamages, DNA-damages, cell death) achieved by down-conversion fluorescent materials such as in conventional organic dye molecules, quantum dots. Once we trigger biological tissues with NIR radiation, due to low autofluorescence (reduce scattering and absorption) background, it can't affect tissues or organisms significantly unlike triggering with UV or visible light. Organic Dyes, fluorescent proteins have drawn our attention in bio-detection but the associated drawbacks – chemical deterioration, low absorption, wide emission spectral range, high photobleaching are limiting their applications though they can possess strong fluorescence intensity. UCNPs with unique ultrasmall physical dimensions, strong UV/visible emissions, higher penetration depth, low photobleaching, sharp emission spectra, high photostability, multimodal imaging have received our tremendous attention by replacing them with organic dyes, quantum dots and fluorescent probes [8,9]. Numerous processes are attributed in lanthanide (Ln) based UCNPs to redistribute the energy within the crystal itself either between sensitizer (S-ion, Yb^{3+}) -to- activator (A-ion, Er^{3+}) or among S-ions ions/A- ions. Excited state absorption (ESA) is known as "photon addition" process resulting in higher energy photon emissions, Energy transfer upconversion (ETU) is an energy transfer process between S-ion and A-ion [10]. The other internal processes – cross relaxations (CR) between two A-ions, energy migration (EM) between two S-ions, radiative or non-radiative relaxations among A-ions appear to be redistributed energy processes – which yield a non-linear response of emissions[11]. However, relatively efficient UC process can only be achieved with a few trivalent lanthanide ions(Nd^{3+}, Sm^{3+},Gd^{3+},Eu^{3+},Er^{3+},Tm^{3+}), so most of the authors preferred to introduce them in fabricating UCNPs for their research work where they act as activator ions and involve strong emissions with 525nm,535nm,600nm,664nm,766nm(Nd^{3+}); 555nm,590nm(Sm^{3+}); 312nm(Gd^{3+});590nm,613nm(Eu^{3+});542nm,655nm(Er^{3+});475nm,800nm(Tm^{3+}) wavelengths [12,13].

The concept of energy-transfer mechanism in UCNPs is sufficiently well established, the erudition on how to create ultrasmall (sub-5nm) with bright NIR-to-UV UCNPs of NaYF4:Yb^{3+}, Er^{3+} systems is still lacking [14-16]. In this work, ultrasmall(sub-5nm) nanoparticles have been designed following a suitable thermal decomposition technique which is modified with the previous research reports [17,18]. The controlled sizes and shapes were achieved with high temperature heat-treatment (300-330 degree C). The preparatory steps were modified incorporating high boiling solvent and surfactant and avoiding long-time heating. This modified method was repeated several times to confirm their controlled sizes. During synthesis, nucleation has taken place followed by the growth of nuclei in nanocrystals. This method controlled the sizes in a relatively short time. By obstructing Ostwald ripening process, 2.5-4.5 nm sized, α-phases of NaYF4:Yb^{3+}, Er^{3+} were formed with heating in ODE/OA (5:2) which (the increased solvent: surfactant ratio) influenced the sizes [19-24]. The lanthanide salt precursors in the ratio of 1.51:1.93:0.19 were used in gram scale. They were dissolved in aqua solution and a respective amount of Y/Yb/Er = 4:1:1 was employed in a one-pot procedure where Ln hexahydrate chloride salts were heated in a mixture of ODE/OA at 300°C for 26 min to obtain ~2.5-4.5 nm size nanoparticles. To the best of our knowledge, till now, NaYF4:Yb^{3+}, Er^{3+} UCNPs have been found to be one of the highly efficient UCNPs [23-25].

Chen et al. reported the UCQY values of 0.13%, 0.07%, 0.05% and 0.95% under 540, 660, 800, and 970 nm NIR excitations, respectively for the UCNPs of size 100 nm (NaYF4:Er^{3+}, Yb^{3+}) [26]. In another study the internal UCQY for core shell UCNPs of size ~ 40 nm (β-NaYF4:Er^{3+} core, dia. 19.2 nm and β-NaLuF4 shell with thickness 18.8 nm) was reported as 3% with 1523 nm NIR laser irradiance [27]. Boyer et al. reported the UCQY for different sizes of UCNPs (NaYF4:Er^{3+}, Yb^{3+}) and their values were 0.005%, 0.10%, 0.30% and 3% for 8-10nm, 30nm,100nm and above 100nm sized UCNPs, respectively, once they were excited with 980 nm NIR laser [28]. Our current synthesized US-UCNPs exhibit higher UCQY in fs-laser irradiation compared to the earlier reports with these ultrasmall sizes (sub5-nm). Importantly, this work also reveals that the US-UCNPs could be a potential candidate for efficient ultraviolet emissions which could be useful as UV-emitting nanophosphors and can be further used in several bio-applications [29,30].

Experimental

Materials and Method

(A) Materials

Materials and Chemicals: The lanthanide precursors were formulated from their corresponding hexahydrate salt solutions such as: Cl3Y:6H2O; Cl3Yb:6H2O Cl3Er:6H2O which were purchased from Sigma –Aldrich and with 99% purity. Technical grade chemical 1- Octadecene (90%), Oleic Acid (65%) NaOH (97.0%), NH4F (95 %) were purchased from sigma Aldrich, Qualigens, SDFCL and Kemphasol, respectively.

(B) Synthesis of US-UCNPs

The specific amount of 1-Octadecene (15 ml), Oleic-acid(6ml) were added in evaporated lanthanide precursors in a three-neck-round-bottom flask kept on a heating mantle. The resulted solution was heated towards higher temperature with both gassed and degassed (vacuum) condition to remove the excess water and oxygen from the solution. The as-prepared solution was brought to highest temperature (300°C) under inert gas (Ar) condition for a very short period of time only and subsequently kept for cooling naturally. Next day the US-UCNPs were collected only by Acetone and isolated via centrifugation and the precipitated sample was kept with dissolving in cyclohexane as they are well dispersed in such non-polar organic solvent.

(C) Characterizations

For characterization of the prepared sample we have performed transmission electron microscopy and high resolution transmission electron microscopy (TEM and HRTEM- FEI TecnaiG2-TWIN 200 KV), Energy Dispersive X-ray analysis(EDXA), X-Ray diffraction pattern (XRD with CoKα- radiation) Raman Spectroscopy (WiTec, alpha 300), Fluorescence Spectrometer (HITACHI, F-4600) provided with an external near infrared (NIR) laser source 980nm to measure the upconversion fluorescence (UCF) spectra, Ti Sapphire tunable oscillator laser with femtosecond pulses to further characterize upconversion emissions.

Results and Discussions

TEM analysis figure 1 (a-e) explicit the formations of ultrasmall nanoparticles in a regular arrangement with no aggregation. Particle-sizes are confined below 5nm with a standard deviation of ±0.9nm (Confirmed by calculating from several low-to-high resolution micrographs). It is clear that the particle sizes vary from ~2.27nm to ~5.2 nm. The interparticle separation has been confirmed to be 5-6.5nm. TEM analysis shows discrete crystalline particles. Average particle size found to be 3.5nm ±0.9nm (TEM histogram analysis figure 1f). The lattice fringes appear to be 3.19nm and confirms the presence of cubic phases (alpha- $NaYF4:Yb^{3+}$, Er^{3+}).

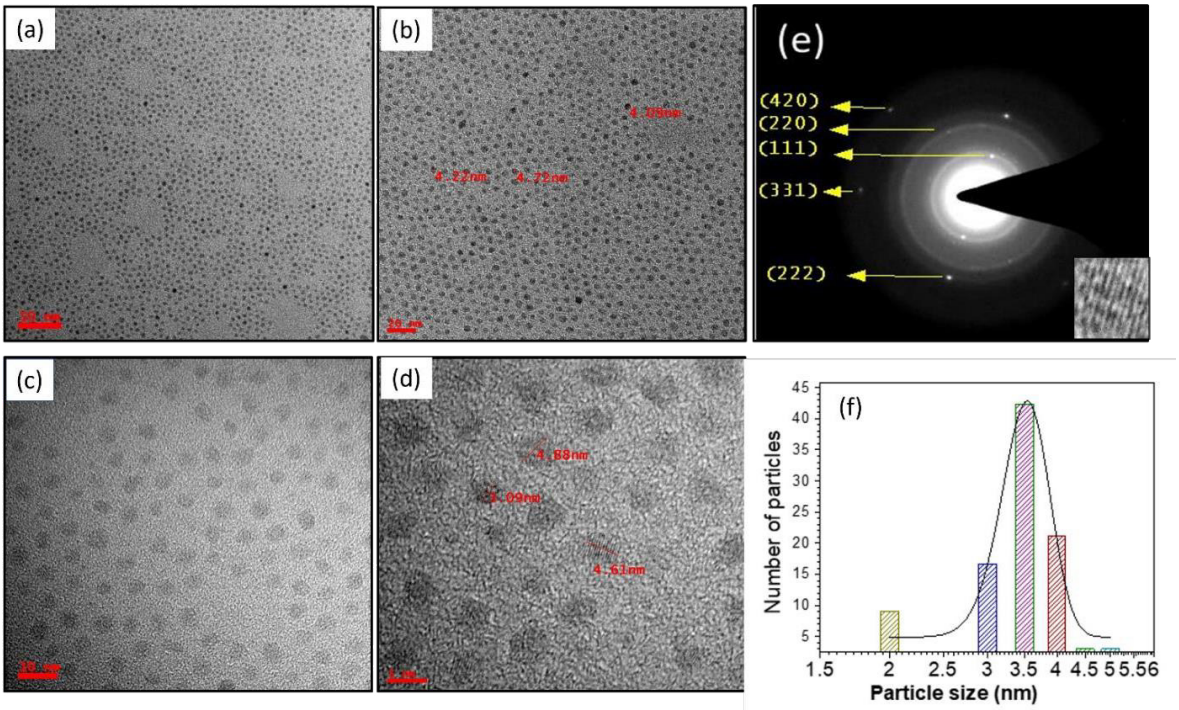

Figure 1: Low Resolution to High Resolution TEM Images of The Synthesized US-UCNPs At Different Magnifications [1a-50nm, 1b- 20nm,1c-10nm, 1d- 5nm] – Uniformly Distributed and Monodispersed in Nature. Panel 1e Represents Crystallinity. Panel If Shows the Histogram Analysis for Particle Sizes Developed in this Work.

The upconversion fluorescence spectra (UCF) spectra have been recorded with 900 nm CW laser diode excitation source and hence, bright blue visible emission[2H9/2(Er^{3+}) - 4I15/2(Er^{3+})] employing three direct energy transfers from sensitizer (Yb^{3+}) to activator ion (Er^{3+}), two non- radiative relaxations within activator ion (Er^{3+}) are observed and described below (Figures 2a,2b) [31-33]:

Step 1: ET1: $2F_{5/2}(Yb^{3+}) + 4I_{15/2}(Er^{3+}) - 2F_{7/2}(Yb^{3+}) + 4I_{11/2}(Er^{3+})$
Step 2: Non radiative relaxation followed by $4I_{11/2}(Er^{3+}) - 4I_{13/2}(Er^{3+})$
Step 3: ET2: $2F_{5/2}(Yb^{3+}) + 4I_{13/2}(Er^{3+}) - 2F_{7/2}(Yb^{3+}) + 4F_{9/2}(Er^{3+})$
Step 4: ET3: $2F_{5/2}(Yb^{3+}) + 4F_{9/2}(Er^{3+}) - 2F_{7/2}(Yb^{3+}) + 4G_{11/2}(Er^{3+})$
Step 5: Non radiative relaxation followed by $4G_{11/2}(Er^{3+}) - 2H_{9/2}(Er^{3+})$ $2H_{9/2}(Er^{3+}) - 4I_{15/2}(Er^{3+})$ = Blue emission (415nm)

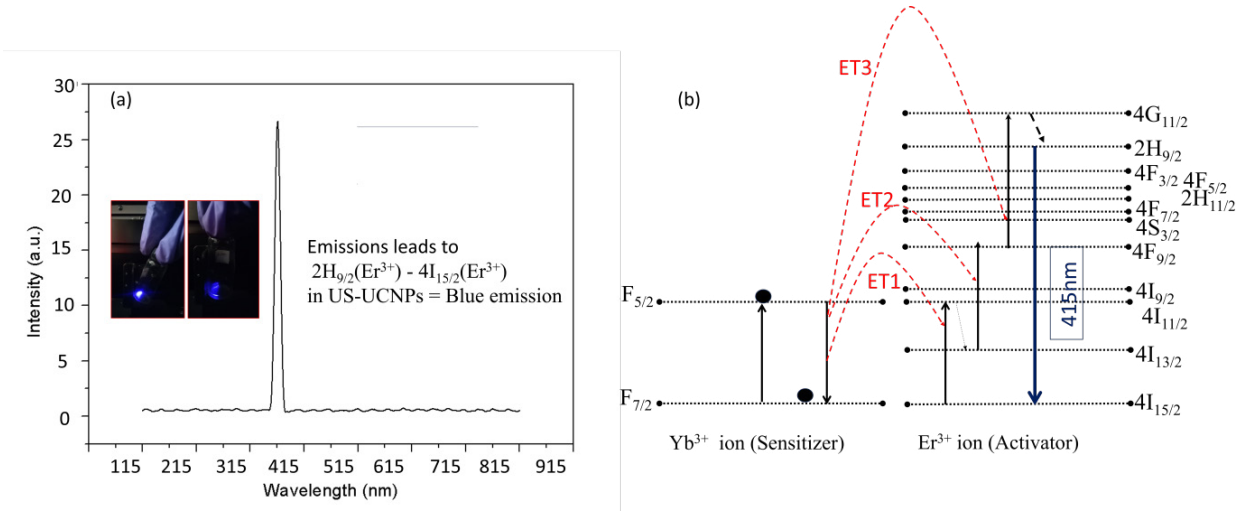

Figure 2: (A) UCF spectra Received From US-UCNPs, Excited With 900nm CW Laser Diode Source, Insets - Blue Emission(415nm) From Synthesized Solution In Cuvette (B) Energy Transfer Mechanism Followed by Three Direct Energy Transfers.

The UCF spectra received with 526/547nm emission, exhibit less intense green visible emissions [$2H_{11/2}$ /$4S_{3/2}$ (Er^{3+}) - $4_{115/2}$ (Er3+)] compared to blue one following two direct energy transfers and one one-radiative relaxation (Figures 3a,3b) [31-33]:
Step 1: ET1- $2F_{5/2}(Yb^{3+}) + 4I1_{5/2}(Er^{3+}) - 2F_{7/2}(Yb^{3+}) + 4I\ (Er^{3+})$
Step 2: ET2- $2F_{5/2}(Yb^{3+}) + 4I_{11/2}(Er^{3+}) - \ 2F_{7/2}(Yb^{3+}) + 4F_{7/2}(Er^{3+})$
Step 3: Non-radiative relaxations followed by:
$4F_{7/2}(Er^{3+}) - 2H_{11/2}\ (Er^{3+})$ (527 nm emission)
$4F_{7/2}(Er^{3+}) - 4S_{3/2}\ (Er^{3+})$ (547 nm emission)

$2H_{11/2}$ /$4S_{3/2}$ (Er^{3+}) - $4I_{15/2}$ (Er^{3+}) = Green emissions(527/547nm).

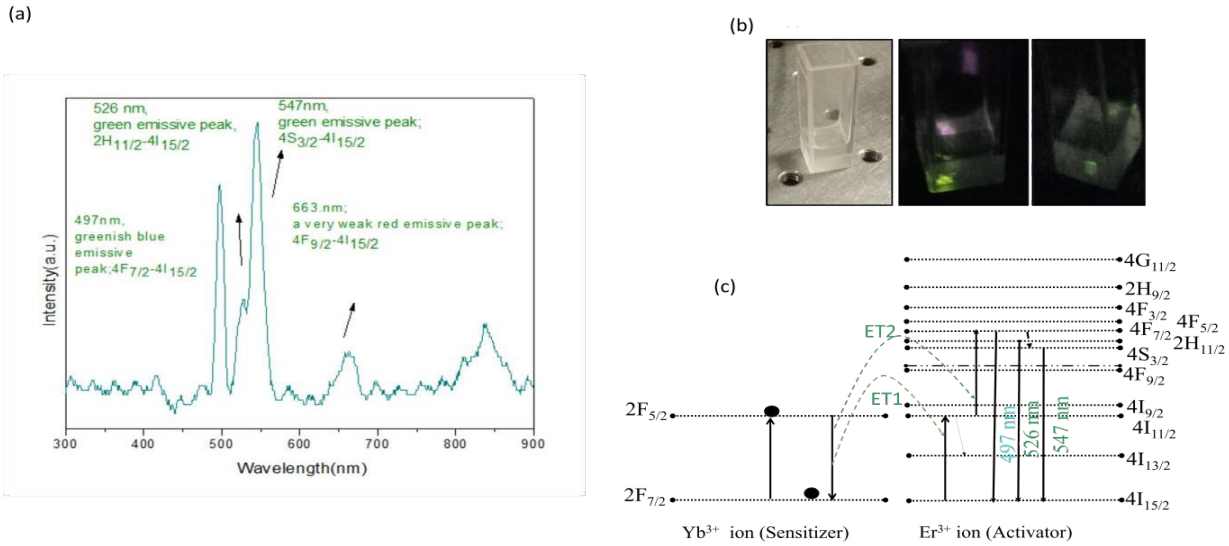

Figure 3: (A) UCF Spectra Received with 980nm Laser Diode Excitation Source, Followed By A Total Of Three Direct Energy Transfers (B) Green Emissions From-Sample-Cuvette (C) Energy Transfer Up Conversion Mechanism Succeeding With 980nm Laser Excitations.

The UCF spectra with 497 nm emission corresponds to the following two direct energy transfers without incorporating any non-radiative relaxation (Figures 3a,3b) [31-33]:
Step 1: ET1- $2F_{5/2}(Yb^{3+}) + 4I_{15/2}(Er^{3+}) - 2F_{7/2}(Yb^{3+}) + 4I_{11/2}(Er^{3+})$
Step 2: ET2- $2F_{5/2}(Yb^{3+}) + 4I_{11/2}(Er^{3+}) - 2F_{7/2}(Yb^{3+}) + 4F_{7/2}(Er^{3+})$
No non-radiative relaxations are followed.
The direct emission $4F_{7/2}(Er^{3+}) - 4I_{15/2}(Er^{3+})$ is responsible for 497 emissions.

However, the results of luminescence with fs-laser interaction can be related and explained well with the generation of non-linear optical second and third order effects in photonic crystals and cavities as surveyed by Aktsipertrov et. Al. group [34] who observed these effects in magnetophotonic crystals (MPCs) fabricated from few layers of Bi:YIG (Bi-substituted with Yttrium) and silica (SiO2) with explaining the second-harmonic generation (SHG) and the third-harmonic generation (THG) in the field of non-linear optics (NO). In view of these features, multiphoton absorption upconversion lasing authorizes prime applications in bioimaging, photodynamic therapy,3D optical data storage.

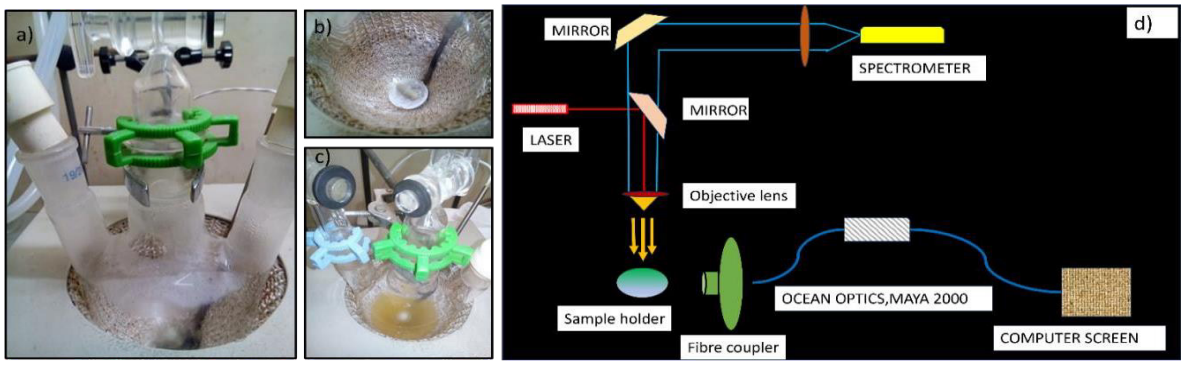

Figure 4: Images (A), (B), (C) Show the Experimental Set-Up During Reaction or Preparation of US-UCNPs in Inert Gaseous Condition and Controlling Several Reaction Parameters At Different Stages. Image (D) A Schematic Set-Up Of Tunable Fs-Laser Employed To Receive MPA.

In the present work, efficient multiphoton absorptions (5 photons/3photons) upconversion lasing from these ultrasmall nanoparticles (US-UCNPs) is perceived at room temperature. Figure 4(a-c) shows the experimental images of synthesized UCNPs at different preparatory steps.

Hence, 140 fs pulses were generated with a fs laser source - pumped with Ti-Sapphire oscillator at a repetition rate of 80 MHz. The pumping light was focused through objective lens. The upconverted emitted signal was also collected by the same lens and finally was detected using sensitive fiber coupled spectrometer.

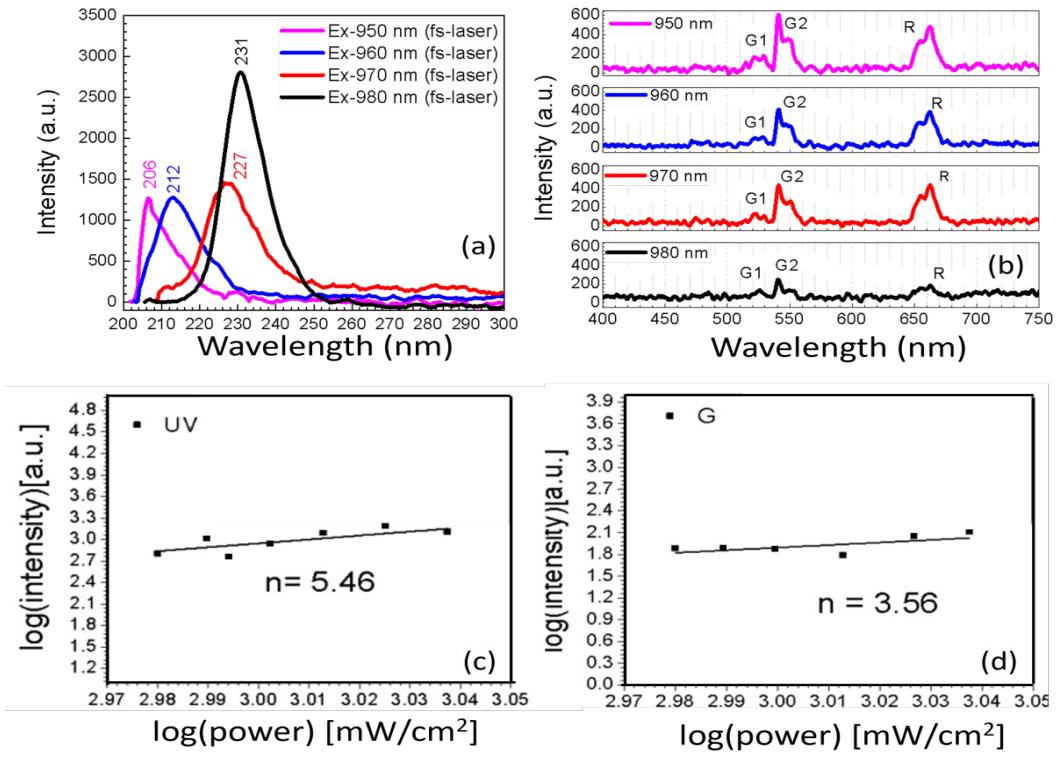

Figure 5: Formations of (A)Dominant Harmonic Lasing Peaks in UV Region (B) Dominated Lasing Peaks In Visible Region; with Fs-Laser Irradiations (C), (D) Show The Evaluated "N" (Numbers Of Absorbed Photons) values for UV, and Green Emissions(G),Respectively

The Power Was Calculated With Optical Power Meter (MAYA 2000, Ocean Optics). A Schematic Of This Experimental Arrangement Is Shown In Figure 4d.

Moreover, the MPA upconversion lasing and higher order peak generation in US-UCNPs under fs-laser pulses are studied. The upconverted peaks exhibit efficient FHG, FIHG appeared for 970nm,980nm, and 950nm,960nm respectively. The higher order harmonic generations are (HHG) occurred along with their appearances as dominant harmonic peaks at 206nm,212nm,227nm,231nm over visible peaks appeared at 521nm,522nm,522nm and 524 nm, respectively (Figures 5a,5b). Figure 5a exhibits a clear red shifting where the central wavelengths of the peaks are shifted from 206 nm to 231nm, significantly. However, the dominated visible peaks are intense enough to be specified (Figure 5b). However, the number of absorbed photons(n) per emitted radiation has been calculated to be 5.46, 3.56 for ultraviolet, green emissions respectively (Figures 5c,5d). The number of absorbed photons is calculated under fs-laser excitation by using the equation: $I_{UC} \sim I_{Fs}$ n [35-37].

Where, I_{UC} = Observed luminescence intensity
n = The number of absorbed photons per emitted photon.
I_{Fs} = Fs-laser excitation power

The upconversion quantum yields (UCQYs) have also been calculated with different excitation power densities of 15.428 W/cm2, 14.154 W/cm2, 13.517 W/cm^2, and 12.739 W/cm2 according to the method reported elsewhere [26,27]. However, in the present study, for visible emissions both external and internal UCQY have been calculated (Figures 6a-6d) and found to be (External-UCQY): 0.121 ± 0.003 %, 0.112±0.002%, 0.105±0.001%, 0.102±0.002%; and (Internal-UCQY): 0.273±0.004%, 0.227±0.002%, 0.192±0.002%, 0.181±0.005%; whereas in

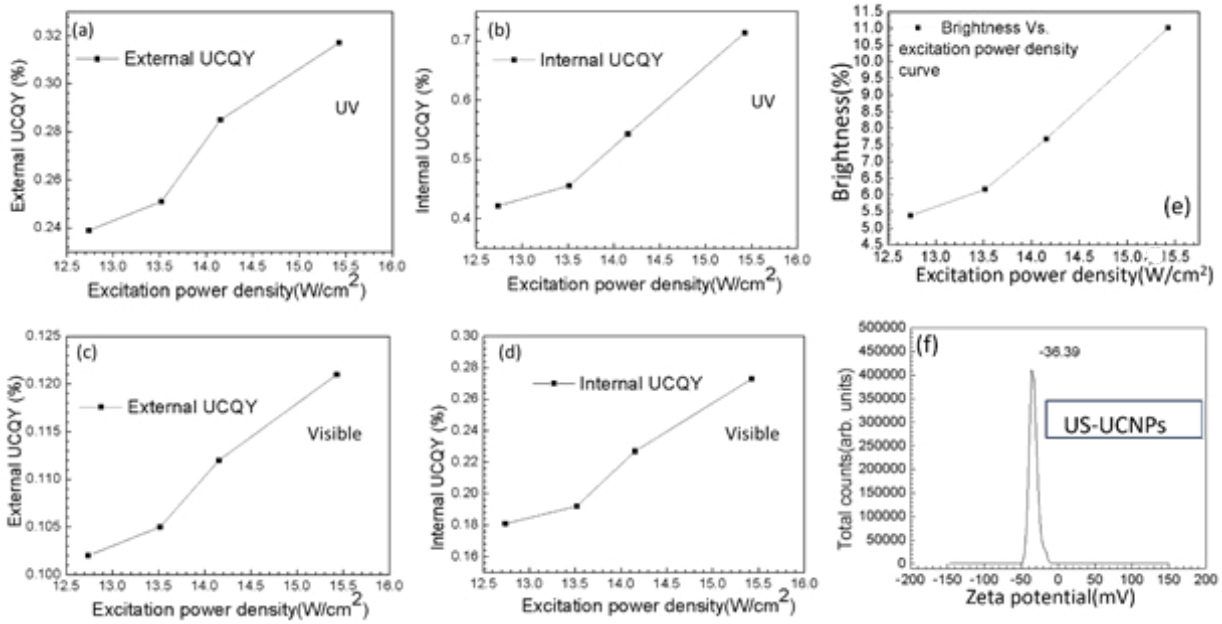

Figure 6: (A) (c) External Quantum Yields and (B), (D) Internal Quantum Yields, With Different Laser Excitation Power Densities, For UV and Green Visible Emissions. (E) A Plot Showing The Variation Of Brightness of US-UCNPs With Varying Laser Excitation Power Densities (F) The Zeta Potential Value for US-UCNPs Found to be -36.30mV Confirm Their Stability.

UV-region they are calculated to be (External-UCQY): 0.317± 0.003%, 0.285 ±0.004%,

0.251±0.002%, 0.239±0.002%; and (Internal-UCQY): 0.714±0.007%, 0.543±0.002%,

0.456±0.001%, 0.422±0.001%, respectively and appear to be efficient while compared with as- said previous observations [26-28,38]. It is also been observed that UCQY increases with increase in the irradiance. The brightness with the excitation power densities for the highly intense UV emissions are plotted in figure 6e.

Further, the intensity ratios for G1/G2; R/G1;(G full=G1+G2) /R; UV/R, UV/G1, UV/G2(G1- 526nm of green emission), G2(547nm of green emission), R (very weak intense red emission) have also been plotted with fs laser excitation wavelengths(λex) and shown in supplementary figure 1(a-d). Based on the excitation pump powers, log(intensity) vs log (excitation powers) plots for UV, G1, G2, red emissions are shown in supplementary figure 2.

Summary And Conclusion

The reduced sizes can produce only a few numbers of emitters(A-ions) in luminescent materials and hence, the

decreased sizes enhance the surface quenching, decrease the number of emitter ions (Er3+ - ions) per particle helping to reduce cross relaxations [39]. Gordon et al. group reported isolating nanocrystals with one activator ion to have limited cross relaxations [40]. Hence, 5 photons,3 photons absorption processes in upconversion emissions (UV, Green) have been demonstrated for the synthesized US-UCNPs. The co-existence of dominant emission peak(visible- region) and higher-order harmonic generation (HHG) are observed with high power fs-laser pulse excitation. It is realized that, the generation of higher order harmonics completes in three steps (i) Incident beam of intense ultrafast radiation induced change in the birefringence or refractive index in the materials (ii)Materials behave like a nonlinear hertzian oscillator and generates polarized waves from the surface or interfaces (ii) the generated polarized waves interact with each other (iii) The interference of polarized waves generates the 4th and 5th harmonics. Here, it is clear to us that both the excitation and emission lines of synthesized US-UCNPs falling into the optical window or therapeutic window (650nm-1350nm), assure maximum tissue penetration depth and allow for low-scattering and bio-detections while the emissions falling into UV direct their extensive applications in Photodynamic therapy (PDT therapy). The toxicity of these nanoparticles has been found to be very less (9.8%). Previously, Vetrone et. al. group reported the uses of fs-NIR pulses in minimizing thermal loading and tissue damages [41]. Another group of researchers applied fs-laser based excitations (1040-1560nm) for in-vivo imaging for deepest penetration depth of about 800µm in a mouse brain [42]. Ji et al group presented a wavelength tunable fs-laser for accurately manipulating optogenetic proteins [43]. However, all these studies are directing the strong applications of synthesized US-UCNPs for those above said applications with NIR-fs-lasing system.

Acknowledgements

Author acknowledges the financial support awarded to M. Das Modak by Department of Science and Technology (DST), Ministry of Science and Technology, Govt of India and Laboratory, instrumentation supported by SEST, ACREHM - HCU. The author must acknowledge TEM operator Mr. Pankaj Kumar for operating TEM instrument very carefully with highly magnified images. M.D. Modak also acknowledges Defence Research and Development Organizations (DRDO), Ministry of Defence, and Government of India (ERIP/ER/1501138/M/01/319/D(RD)) for providing fs-laser facility.

References

1. Ajee, R. S., Roy, P. S., Dey, S., & Sundaresan, S. (2024). Upconversion nanoparticles and their potential in the realm of biomedical sciences and theranostics. Journal of Nanoparticle Research, 26(3), 50.
2. Kaplan, M., & Uzun, L. (2025). Upconversion nanoparticles in biomedical applications: Its potential for early diagnosis of cancer and telomeric activity. Journal of Pharmaceutical and Biomedical Analysis Open, 5, 100049.
3. Yadav, N., & Khare, A. (2023). Applications of Upconversion Nanoparticles for Solar Cells. In Upconversion Nanoparticles (UCNPs) for Functional Applications (pp. 339-367). Singapore: Springer Nature Singapore.
4. Gao, L., Shan, X., Xu, X., Liu, Y., Liu, B., Li, S., ... & Wang, F. (2020). Video-rate upconversion display from optimized lanthanide ion doped upconversion nanoparticles. Nanoscale, 12(36), 18595-18599.
5. Wang, C., Cheng, L., & Liu, Z. (2013). Upconversion nanoparticles for photodynamic therapy and other cancer therapeutics. Theranostics, 3(5), 317.
6. S. Bian, W. Lu, L. Zhou, T. Jin, Mater Today Commun 41(2024)110301.
7. Mirmajidi, H., Lee, H., Nipu, N., Thomas, J., Gajdosechova, Z., Kennedy, D., ... & Hemmer, E. (2025). Nano-bio interactions of Gum Arabic-stabilized lanthanide-based upconverting nanoparticles: in vitro and in vivo study. Journal of Materials Chemistry B, 13(1), 160-176.
8. Dubey, N., & Chandra, S. (2022). Upconversion nanoparticles: Recent strategies and mechanism based applications. Journal of Rare Earths, 40(9), 1343-1359.
9. Eraky, M. S., Elsherif, S. S., & Sanad, M. M. (2025). Recent Trends in Upconversion Luminescent Inorganic Materials and Nanomaterials for Enhanced Photovoltaic Solar Cell and Biological Applications. Journal of Fluorescence, 1-25.
10. Das Modak, M., & Paik, P. (2020). A Wide Portray of Upconversion Nanoparticles: Surface Modification for Bio-applications. In Immobilization Strategies: Biomedical, Bioengineering and Environmental Applications (pp. 335-369). Singapore: Springer Singapore.
11. Kotulska, A. M., Pilch-Wróbel, A., Lahtinen, S., Soukka, T., & Bednarkiewicz, A. (2022). Upconversion FRET quantitation: the role of donor photoexcitation mode and compositional architecture on the decay and intensity based responses. Light: Science & Applications, 11(1), 256.
12. Dong, H., Sun, L. D., & Yan, C. H. (2015). Energy transfer in lanthanide upconversion studies for extended optical applications. Chemical Society Reviews, 44(6), 1608-1634.
13. Li, X., Zhang, F., & Zhao, D. (2015). Lab on upconversion nanoparticles: optical properties and applications engineering via designed nanostructure. Chemical Society Reviews, 44(6), 1346-1378.
14. T. Joshi, C. Mamat, H. Stephan, Chemistry Open 9 (2020) 703-712.
15. Liu, D., Yan, J., Wang, K., Wang, Y., & Luo, G. (2022). Continuous synthesis of ultrasmall core-shell upconversion nanoparticles via a flow chemistry method. Nano Research, 15(2), 1199-1204.
16. Zhang, Y., Yu, Z., Li, J., Ao, Y., Xue, J., Zeng, Z., ... & Tan, T. T. Y. (2017). Ultrasmall-superbright neodymium-upconversion nanoparticles via energy migration manipulation and lattice modification: 808 nm-activated drug release. ACS nano, 11(3), 2846-2857.
17. Boyer, J. C., Cuccia, L. A., & Capobianco, J. A. (2007). Synthesis of colloidal upconverting NaYF4: Er3+/Yb3+ and Tm3+/Yb3+ monodisperse nanocrystals. Nano letters, 7(3), 847-852.
18. Boyer, J. C., Vetrone, F., Cuccia, L. A., & Capobianco, J. A. (2006). Synthesis of colloidal upconverting NaYF4

nanocrystals doped with Er3+, Yb3+ and Tm3+, Yb3+ via thermal decomposition of lanthanide trifluoroacetate precursors. Journal of the American Chemical Society, 128(23), 7444-7445.
19. Rinkel, T., Nordmann, J., Raj, A. N., & Haase, M. (2014). Ostwald-ripening and particle size focussing of sub-10 nm NaYF 4 upconversion nanocrystals. Nanoscale, 6(23), 14523-14530.
20. Niu, W., Wu, S., & Zhang, S. (2011). Utilizing the amidation reaction to address the "cooperative effect" of carboxylic acid/amine on the size, shape, and multicolor output of fluoride upconversion nanoparticles. Journal of Materials Chemistry, 21(29), 10894-10902.
21. Ostrowski, A. D., Chan, E. M., Gargas, D. J., Katz, E. M., Han, G., Schuck, P. J., ... & Cohen, B. E. (2012). Controlled synthesis and single-particle imaging of bright, sub-10 nm lanthanide-doped upconverting nanocrystals. ACS nano, 6(3), 2686-2692.
22. Hesse, J., Klier, D. T., Sgarzi, M., Nsubuga, A., Bauer, C., Grenzer, J., ... & Stephan, H. (2018). Rapid Synthesis of Sub-10 nm Hexagonal NaYF4-Based Upconverting Nanoparticles using Therminol® 66. ChemistryOpen, 7(2), 159-168.
23. Gunaseelan, M., Yamini, S., Kumar, G. A., & Senthilselvan, J. (2018). Highly efficient upconversion luminescence in hexagonal NaYF4: Yb3+, Er3+ nanocrystals synthesized by a novel reverse microemulsion method. Optical Materials, 75, 174-186.
24. Ferrera-González, J., Francés-Soriano, L., González-Béjar, M., & Pérez-Prieto, J. (2023). Engineering of Upconversion Nanoparticles for Better Efficiency. In Upconversion Nanoparticles (UCNPs) for Functional Applications (pp. 19-46). Singapore: Springer Nature Singapore.
25. Mai, H. X., Zhang, Y. W., Sun, L. D., & Yan, C. H. (2007). Highly efficient multicolor up-conversion emissions and their mechanisms of monodisperse NaYF4: Yb, Er core and core/shell-structured nanocrystals. The Journal of Physical Chemistry C, 111(37), 13721-13729.
26. Chen, G., Ohulchanskyy, T. Y., Kumar, R., Ågren, H., & Prasad, P. N. (2010). Ultrasmall monodisperse NaYF4: Yb3+/Tm3+ nanocrystals with enhanced near-infrared to near-infrared upconversion photoluminescence. ACS nano, 4(6), 3163-3168.
27. Fischer, S., Johnson, N. J., Pichaandi, J., Goldschmidt, J. C., & van Veggel, F. C. (2015). Upconverting core-shell nanocrystals with high quantum yield under low irradiance: On the role of isotropic and thick shells. Journal of applied physics, 118(19).
28. Boyer, J. C., & Van Veggel, F. C. (2010). Absolute quantum yield measurements of colloidal NaYF 4: Er3+, Yb3+ upconverting nanoparticles. Nanoscale, 2(8), 1417-1419.
29. Chien, Y. H., Chan, K. K., Yap, S. H. K., & Yong, K. T. (2018). NIR-responsive nanomaterials and their applications; upconversion nanoparticles and carbon dots: a perspective. Journal of Chemical Technology & Biotechnology, 93(6), 1519-1528.
30. Paik, P., Kumar, K. S., Modak, M. D., Kumar, K., & Maity, S. (2018). UCN–SiO 2–GO: a core shell and conjugate system for controlling delivery of doxorubicin by 980 nm NIR pulse. RSC advances, 8(65), 37492-37502.
31. Song, H., Sun, B., Wang, T., Lu, S., Yang, L., Chen, B., ... & Kong, X. (2004). Three-photon upconversion luminescence phenomenon for the green levels in Er3+/Yb3+ codoped cubic nanocrystalline yttria. Solid state communications, 132(6), 409-413.
32. Suyver, J. F., Grimm, J., Krämer, K. W., & Güdel, H. U. (2005). Highly efficient near-infrared to visible up-conversion process in NaYF4: Er3+, Yb3+. Journal of Luminescence, 114(1), 53-59.
33. Suyver, J. F., Grimm, J., Van Veen, M. K., Biner, D., Krämer, K. W., & Güdel, H. U. (2006). Upconversion spectroscopy and properties of NaYF4 doped with Er3+, Tm3+ and/or Yb3+. Journal of Luminescence, 117(1), 1-12.
34. Aktsipetrov, O. A., Dolgova, T. V., Fedyanin, A. A., Murzina, T. V., Inoue, M., Nishimura, K., & Uchida, H. (2005). Magnetization-induced second-and third-harmonic generation in magnetophotonic crystals. Journal of the Optical Society of America B, 22(1), 176-186.
35. Kingsley, J. D., Fenner, G. E., & Galginaitis, S. V. (1969). KINETICS AND EFFICIENCY OF INFRARED-TO-VISIBLE CONVERSION IN LaF3: Yb, Er. Applied Physics Letters, 15(4), 115-117.
36. Lu, D., Cho, S. K., Ahn, S., Brun, L., Summers, C. J., & Park, W. (2014). Plasmon enhancement mechanism for the upconversion processes in NaYF4: Yb3+, Er3+ nanoparticles: Maxwell versus Forster. ACS nano, 8(8), 7780-7792.
37. Suyver, J. F., Aebischer, A., García-Revilla, S., Gerner, P., & Güdel, H. U. (2005). Anomalous power dependence of sensitized upconversion luminescence. Physical Review B—Condensed Matter and Materials Physics, 71(12), 125123.
38. Hatami, S., Würth, C., Kaiser, M., Leubner, S., Gabriel, S., Bahrig, L., ... & Resch-Genger, U. (2015). Absolute photoluminescence quantum yields of IR26 and IR-emissive Cd 1− x Hg x Te and PbS quantum dots–method-and material-inherent challenges. Nanoscale, 7(1), 133-143.
39. Amouroux, B., Eftekhari, A., Roux, C., Micheau, J. C., Roblin, P., Pasturel, M., ... & Coudret, C. (2024). Synthesis and Emission Dynamics of Sub-3 nm Upconversion Nanoparticles. Advanced Optical Materials, 12(24), 2303283.
40. Alizadehkhaledi, A., Frencken, A. L., van Veggel, F. C., & Gordon, R. (2019). Isolating nanocrystals with an individual erbium emitter: A route to a stable single-photon source at 1550 nm wavelength. Nano Letters, 20(2), 1018-1022.
41. Vetrone, F., Naccache, R., de la Fuente, A. J., Sanz-Rodríguez, F., Blazquez-Castro, A., Rodriguez, E. M., ... & Capobianco, J. A. (2010). Intracellular imaging of HeLa cells by non-functionalized NaYF4: Er 3+, Yb 3+ upconverting nanoparticles. Nanoscale, 2(4), 495-498.
42. Zheng, Z., Li, D., Liu, Z., Peng, H. Q., Sung, H. H., Kwok, R. T., ... & Tang, B. Z. (2019). Aggregation-induced nonlinear optical effects of aiegen nanocrystals for ultradeep in vivo bioimaging. advanced materials, 31(44), 1904799.

43. Ji, W., Wang, S., Zhao, J., Tian, Y., Pan, H., Zheng, B., ... & Chang, J. (2019). Accurate manipulation of optogenetic proteins with wavelength tunable femtosecond laser system. Journal of Applied Physics, 125(16).